A Thesis

On

Study on room temperature ferromagnetic behavior of Tb doped ZnO nanoparticles

Submitted in partial fulfillment of the requirement for the award of the degree of

Master of Science (Physics)

Submitted by
Amita Pal
Roll No: 300904003

Supervisor
Dr. N. K. Verma

Senior Professor of Physics

Under

School of Physics and Materials Science

Thapar University, Patiala-147 004
July 2011

Certificate

This is to certify that the report entitled **"Study on room temperature ferromagnetic behavior of Tb doped ZnO nanoparticles"** submitted by **Ms. Amita Pal (300904003)** of **M.Sc (Physics),** Thapar University, Patiala was carried out by her under my supervision. She has not submitted this material for credit towards any other degree at Thapar University, Patiala or any other University.

(Dr. N.K. Verma)

Senior Professor

School of Physics and Materials Science

Thapar University, Patiala

(Dr. O. P. Pandey)

Professor and Head

School of Physics and Materials Science

Thapar University, Patiala

(Dr. S. K. Mohapatra)

Dean of Academic Affairs

Thapar University, Patiala

Acknowledgement

I express my deep sense of gratitude and respect to my guide **Dr. N K Verma, Senior Professor, School of Physics and Materials Science, Thapar University, Patiala** for his keen interest and valuable guidance, strong motivation and constant encouragement during the course of the work. I thank him from the bottom of my heart for introducing me to Nanotechnology. I thank him for his great patience, constructive criticism and many useful suggestions apart from invaluable guidance to me. I am sure that the knowledge gained through my association with my supervisor will help me in future.

I am thankful to **Mr. Gurmeet Singh Lotey** for their kind help and suggestions at every stage of my project report work.

I am also thankful to Mr.Sanjeev Kumar, Ms.Manveen Kaur, Ms.Lavanya Khana and Mr.Jaspal Singh for their help and support at every stage during the project report work.

Finally, I would like to express my deepest gratitude to **my parents,** without whom I am nothing, to provide me great opportunities, everlasting support, big encouragement and lots of love.

(Ms. Amita Pal)

Abstract

The prospect of a new generation of electronic devices based on the fundamental quantum property of angular momentum, known as spin, has led to the rapidly developing field of spintronics. It is envisioned that these advanced devices will have significant advantages over traditional charge based electronics in properties such as speed, power consumption and long coherence times. Diluted magnetic semiconductors (DMS) are one of the most promising candidates for spintronic application are considered a promising system for exhibiting spintronic functionality. These materials are created by using molecular beam epitaxy (MBE) to incorporate into traditional semiconductors a quantity of transition metal atoms sufficient that ferromagnetism is exhibited.

The $Zn_{1-x}Tb_xO$ with $x \leq 0.05$, nanoparticles were prepared by chemical co-precipitation method. The samples were characterized through x-ray diffractometer (XRD) for structural and phase analysis. The optical properties of synthesized Tb-doped ZnO nanoparticles were studied by UV-Visible spectroscopy. The magnetic studies were done by vibrational sample magnetometer (VSM). The pure ZnO nanoparticles show ferromagnetic behaviour and with doping of Tb, it changes to antiferromagnetic. The remnant magnetisation m_r is 2.69×10^{-5} emu/g and coercive field is 2019.43 Oe observed for pure ZnO nanoparticles.

List of Figures Page No.

Contents: Page No.

4.5 Characterization Techniques **Page No.**

1.1 Nanomaterials

Nanomaterials are defined as materials composed of one or more engineered nano-components. A nano-component has at least one of its dimensions between 1nm and 100nm. These nano-components or their interactions are engineered to impart the unique properties of these materials. Examples include nanotubes, nanoparticles, nanostructured materials, and designer molecules. These materials have the potential for wide-ranging industrial, biomedical, and electronic applications. Nanomaterials can be metals, ceramics, polymeric materials, or composite materials. Their defining characteristic is a very small feature size in the range of 1-100 nanometers (nm). One nanometer spans 3-5 atoms lined up in a row. Two principal factors cause the properties of nanomaterials to differ significantly from other materials:

- Increased relative surface area
- Quantum effects.

These factors can change or enhance properties such as reactivity, strength and electrical properties, optical characteristics.

Nanomaterials find Application in following fields

- **Cosmetics application of nanoparticle: S**unscreen lotions: ray absorb properties.
- **Nanocomposite materials:** Nanoparticle silicate nanolayer (clay nanocomposites) and nanotubes can be used as reinforzed filler not only to increase mechanical properties of nanocomposites but also to impart new properties (optical, electronic etc.)
- **Nanocoatings:** Surface coating with nanometre thickness of nanomaterial can be used to improve properties like wear and scratch-resistant, optoelectonic.
- **Hard cutting tools:** Current cutting tools (e.g. mill machine tools) are made using a sort of metal nanocomposites such as tungsten carbide, tantalum carbide and titanium carbide that have more wear and erosion-resistant, and last longer than their conventional (large-grained) materials.
- **More performed paint**: Using nanoparticles to improve paint properties.
- **Fuel cells:** Could use nano-engineered membranes to catalytic processes for improve efficiency of small-scale fuel cells.

- **Displays:** New class of display using carbon nanotubes as emission device for the next generation of monitor and television (FED field-emission displays).
- **Nanoparticles can be used as fuel additivities** and catalytic more efficient materials.

1.2 Dilute magnetic materials (DMS)

Any semiconductor in which a part of the lattice is replaced by magnetic ions can be regarded as a diluted magnetic semiconductor.The materials are commonly known as semimagnetic semiconductors (SMSC) or diluted magnetic semiconductors (DMS). These mixed crystals (semiconductor alloys) may be considered as containing two interacting subsystems. The first of these is the system of delocalised conduction and valence band electrons. The second is the random, diluted system of localised magnetic moments associated with the magnetic atoms. The most common DMS are II-VI compounds (like CdTe, ZnSe, CdSe, CdS, etc.), with transition metal ions (e.g. Mn, Fe or Co) substituting their original cations. There are also materials based on IV-VI (e.g. PbTe, SnTe) and recently III-V (e.g. GaAs, InSb) crystals. On the other hand, rare earth elements (e.g. Eu, Gd, Er) are also used as magnetic atoms in DMS.

Diluted magnetic semiconductors (DMS) are one of the most promising candidates for spintronic application. The research on the DMS materials which has been carried out worldwide in the past decade has been reviewed in this thesis.DMS material can be realized when a conventional host semiconductor, such as GaAs, ZnO, etc., is doped with magnetic impurities, usually transition metal ions. For practical application, DMS material should favorably be ferromagnetic at room temperature. Early studies on DMS materials showed that ferromagnetic can be induced in Mn doped III-V semiconductors. However, these materials are not suitable for practical applications as their curie temperatures are quite low. On the other hand, some theoretical works predicted room temperature ferromagnetism in transition metal doped oxide semiconductors. This fact has boosted research in the field of DMS materials. The number of reports on observations of room temperature ferromagnetic in Co, Mn, Ni, and Cr doped ZnO and TiO_2 semiconducting oxides are constantly growing.

DMS materials show room temperature ferromagnetism

- III-V group element : GaMnAs , GaMnN , GaMnP, InMnAs
- II-VI group element : ZnMnSe , ZnCrTe , ZnCrSe , CdMnTe ,CdMnSe
- IV-VI group element : PbMnTe, PbSnMnTe
- IV group element : GeMn, SiMnC
- Oxides: : ZnO:Mn, ZnO:Co, TiO_2:Co, SnO_2:Co, Cu_2O:Co
- Others: : $CdGeMnP_2$, $ZnGeMnP_2$, ZnSnMnAs

The prospect of a new generation of electronic devices based on the fundamental quantum property of angular momentum, known as spin, has led to the rapidly developing field of spintronics. It is envisioned that these advanced devices will have significant advantages over traditional charge based electronics in properties such as speed, power consumption and long coherence times. DMS are considered a promising system for exhibiting spintronic functionality. These materials are created by using molecular beam epitaxy (MBE) to incorporate into traditional semiconductors a quantity of transition metal atoms sufficient that ferromagnetism is exhibited. The mechanism responsible for ferromagnetism in III–V magnetic semiconductors is known as the *sp-d* exchange interactions of the band carriers with localized magnetic ions.

Applications of DMS materials

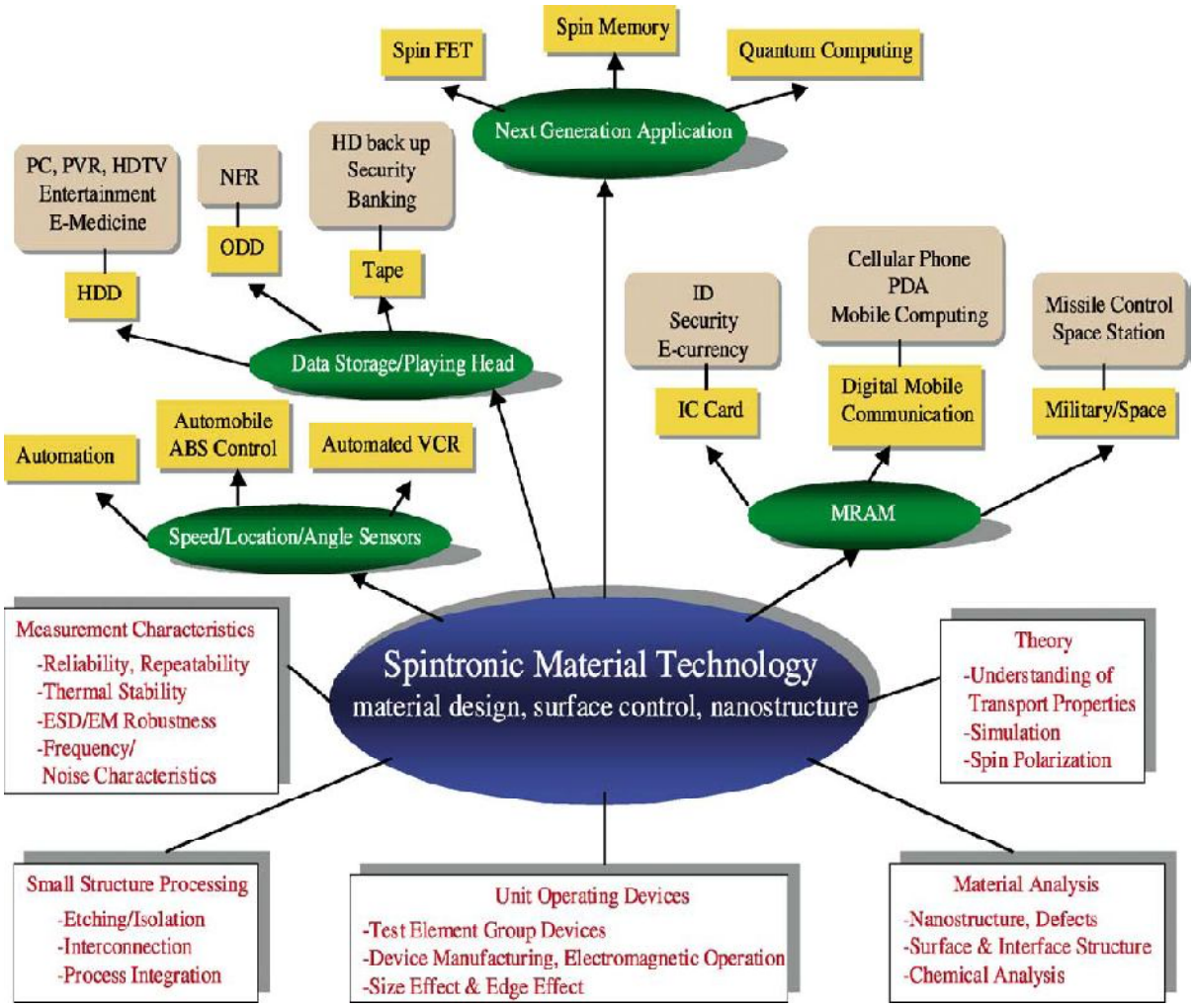

Figure1.1: The various applications of DMS

DMS materials posses following properties

- The semiconductor properties of DMS such as band gap, conductivity, effective mass can be varied in a controlled manner by varying the composition.
- They show phenomenon like room temperature ferromagnetism (RTF), Kerr effect, Resonance Tunneling Behavior, Anomalous Hall Effect, Super-Paramagnetism etc.

DMS materials can be utilized for making chips which can store data in terms of the magnetic spins of the dopant atom. Hence both the charge and spin of the electrons can be effectively utilized in the data storage phenomenon. The various applications of DMS is shown in figure 1.1

1.3 Oxide Dilute Magnetic Semiconductor (ODMS)

The magnetic oxide semiconductor as oxide semiconductor based DMS to provide Tc above room temperature. Among the oxide semiconductors ZnO and TiO_2, have been most extensively studied. There have been many reports on the fabrication of transition-metal doped ZnO or TiO_2. Both bulk and thin film specimens have been synthesized. ZnO has been doped with various transition metals, whereas TiO_2 has been doped mostly with cobalt.

1.3.1Theory of ferromagnetism in ODMS

Despite recent experimental success, a fundamental description of ferromagnetism in DMS remains incomplete. Recent theoretical treatment has yielded useful insight into fundamental mechanisms. Dietl et. al. [1,2] have applied Zener's model for ferromagnetism, driven by exchange interaction between carriers and localized spins to explain the ferromagnetic transition temperature in III-V and II-VI compound semiconductors. The theory assumes that ferromagnetic correlations are mediated by holes from shallow acceptors in a matrix of localized spins in a magnetically doped semiconductor. In another word, the magnetic ions substituted on the group II or III site provide the local spin. When transition metal (TM) is explicitly doped into semiconductor, the open shell of the transition metal gives the localized magnetization. Usually the localized magnetization on TM sites could not couple each other because of the averaged long separation distance. However, the carriers induced by the defects of semiconductor usually show more delocalization in the space. If the magnetized TM shows ferromagnetism, the ferromagnetic coupling between TMs can be mediated by the carriers of the system. Ferromagnetism mediated by carriers in semiconductors is dependent on the magnetic dopant concentration, the carrier type and carrier density. These systems can be envisioned as approaching a metal-insulator transition when carrier density is increased and ferromagnetism is observed. Most of these models describing ferromagnetism are based

on the assumption that the transition metal ions are randomly substituted on the cation sites where they act as the acceptors. Therefore, the carrier density can be significantly lower than the dopant density under these conditions; the exchange interaction among the nearest transition metal ions is mediated by the carrier and gives rise to ferromagnetism in ODMS. Meanwhile, the holes in extended or weakly localized states could mediate the long-range interactions among localized spins. It suggests that for doped semiconducting oxides, carrier mediated ferromagnetism interaction may be possible [3]. Besides carrier mediated ferromagnetism, bound magnetic polaron [4], double exchange and virtual transition [5] are also the theoretical models to explain ferromagnetism. The bound magnetic polaron model, many localized spins due to the transition metal ions interact with a much lower number of weakly bound carriers, leading to polarons. The extent of these polarons increases as the temperature is lowered and the transition temperature occurs essentially when the polaron size is the same as that of the sample. The overlapping of the individual polarons produces longer polarization. This model is inherently attractive for low carrier density systems, such as electronic oxides. The polaron model is applicable to both p- and n-type host materials [6].The double exchange mechanism arising from hopping among the different oxidation states of doped transition metals. The spin glass state is stabilized with the transition metal in the d5 configurations.

The ferromagnetism arises from a competition between the double exchange interactions and the anti-ferromagnetic super-exchange interaction in these materials. While the last model of virtual excitations suggests that the magnetic dopant is excited to the valence band and this could produce the requisite p-d exchange needed for the ferromagnetism in the absence of a large density of free carriers [5]. Diluted magnetic semiconductors are materials whose magnetic properties are strongly influenced by disorder systems. Disorder is an essential ingredient of the magnetic phenomena. Disorder is inherent in all materials, due to randomly placed impurity atoms and can lead to quite different physical phenomenon from that observed in its absence. It is however not surprising to expect the formation of impurity phases or clustering formation of the transition metals in the semiconductor lattices. If this is the case, the mechanism for the ferromagnetism is different and magnetism is not necessarily carrier mediated [3].

1.3.2 Advantages and challenges of ODMS

Driven by the thrust for faster and denser integrated circuits, magnetic semiconductor technology has experienced a continuous reduction in its working dimension, which now has

reached a few tens of atomic spacing. Spin carriers become increasingly important in these small structures because the exchange interaction can become appreciable. From the advanced small features, new spin devices have more and more advantages, such as increased data processing speed, decreased electric power consumption, increased integration densities compared to the conventional semiconductor devices and non-volatility. However, fabrication of intrinsic ODMS remains the major problem for researchers.

The challenges in this field of spintronics include the optimization of electron spin lifetime, the detection of the spin coherence in nanoscale structures, transport of spin-polarised carriers across relevant length scales and manipulation of both electron and nuclear spin on sufficiently fast time scales [7]. In order to overcome the problems and use the spin degree of freedom in semiconductors, one has to be able to create, sustain, control and detect the spin polarization of carriers. The most straightforward way to create and sustain spin polarization electronically is by 'spin injection'. There are a few methods for the spin injection introduced by Wolf et al. [7]: Ohmic injection, tunnel spin injection, ballistic electron injection and hot electron injection. To do this with ferromagnetic metals or semiconductors is not easy. It is because of the presence of scattering at the interface. A very good interface between ferromagnetic and semiconductor is critical for spintronic applications. To control the spin, carrier-induced ferromagnetism might be used. By using field effect to control the carrier density, the ferromagnetism may be turned on and off in a manageable way. The last challenge would be the detection of the spin. Detection requires the spin-selective junction, which can be provided by ferromagnetic materials with a good interface to semiconductors. It is envisioned that the merging of electronics, photonics and magnetics will ultimately lead to a new spin-based multi-functional devices in the near future. If we can understand and control the spin degree of freedom in semiconductor heterostructures and ferromagnets, the potential for high-performance spin based electronics will be high.

1.4 Zinc oxide as diluted magnetic semiconductors

In recent years, magnetically doped ZnO has emerged as a possible DMS material, because theoretical calculations have predicted an above room temperature *T*c. However, experimental results on ZnO-based materials are still controversial. In addition to ferromagnetism, non-ferromagnetic states, such as spin-glass, antiferromagnetism, and paramagnetism, have also been reported. Furthermore, the origin of the ferromagnetism in ZnO-based DMS materials is still controversial, unlike the DMS materials mentioned above

such as GaAs:Mn. Some researchers reported clustering or secondary phase formation as the origin of the ferromagnetism (i.e. an extrinsic mechanism), while others concluded that an intrinsic carrier-mediated mechanism was responsible for the ferromagnetism. In order to experimentally investigate and prove the presence of intrinsic carrier- mediated ferromagnetism in ZnO, some advanced experiments have been recently designed. For example, studies on ZnO co-doped with a transition metal and either a donor or acceptor dopant, such as Zn interstitials, Al, and Ga for *n*-type conduction and N, P, and As for *p*-type conduction, have been pursued to check the role of the free carriers in the ferromagnetism in ZnO-based DMS materials. Furthermore, electrical transport and optical probes beyond the more common techniques for studying magnetism (e.g., bulk magnetization), such as anomalous Hall Effect (AHE) and magnetic circular dichroism, were performed on ZnO-based DMS materials to help distinguish between intrinsic and extrinsic mechanisms of ferromagnetism.

Properties of ZnO

Molecular formula	ZnO
Molar mass	81.408g/mol
Appearance	white solid
Odour	odourless
Density	5.606g/cm^3
Melting point	1975°C
Boiling point	2360°C
Solubility in water	0.16mg/100ml (30°C)
Bandgap	3.3ev (direct)

Zinc Oxide (ZnO) has been widely studied for its attractive applications in ultraviolet light-emitting diodes and laser diodes, because it has a direct bandgap of 3.37 eV at room temperature and a large exciton binding energy of 60 meV. Zinc oxide is an inorganic compound with the formula ZnO. It usually appears as a white powder, nearly insoluble in water. The powder is widely used as an additive into numerous materials and products including plastics, ceramics, glass, cement, rubber (e.g., car tires), lubricants, paints, ointments, adhesives, sealants, pigments, foods (source of Zn nutrient), batteries, ferrites, fire

retardants, first aid tapes, etc. ZnO is present in the Earth's crust as the mineral zincite; however, most ZnO used commercially is produced synthetically. ZnO is a wide-bandgap semiconductor of the II-VI semiconductor group (since zinc and oxygen belong to the 2nd and 6th groups of the periodic table, respectively). The native doping of the semiconductor (due to oxygen vacancies) is n-type. This semiconductor has several favorable properties: good transparency, high electron mobility, wide bandgap, strong room-temperature luminescence, etc. Those properties are already used in emerging applications for transparent electrodes in liquid crystal displays and in energy-saving or heat-protecting windows, and electronic applications of ZnO as thin-film transistors and light-emitting diodes are forthcoming as of 2009. Zinc oxide crystallizes in three forms: hexagonal wurtzite , cubic zincblende, and the rarely observed cubic rocksalt as shown in figure 1.2. The wurtzite structure is most stable at ambient conditions and thus most common. The zincblende form can be stabilized by growing ZnO on substrates with cubic lattice structure. In both cases, the zinc and oxide centers are tetrahedral. Hexagonal and zincblende polymorphs have no inversion symmetry (reflection of a crystal relatively any given point does not transform it into itself). This and

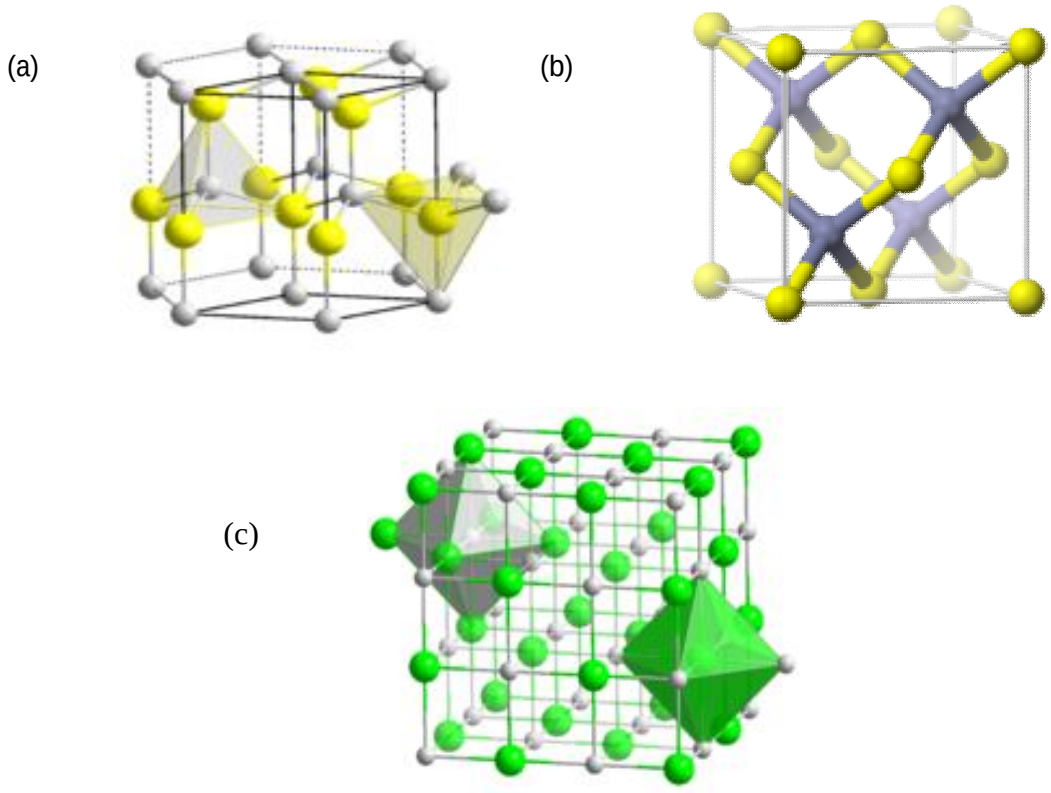

Figure1.2: 3d model of the structure of Wurtzite (a), Zincblende (b) and Rocksalt (c)

other lattice symmetry properties result in piezoelectricity of the hexagonal and zincblende ZnO, and in pyroelectricity of hexagonal ZnO. The lattice constants are a = 3.25 Å and c = 5.2 Å; their ratio c/a ~ 1.60 is close to the ideal value for hexagonal cell c/a = 1.633. [14] As in most group II-VI materials, the bonding in ZnO is largely ionic, which explains its strong piezoelectricity. Due to the polar Zn-O bonds, zinc and oxygen planes bear electric charge (positive and negative, respectively). Therefore, to maintain electrical neutrality, those planes reconstruct at atomic level in most relative materials, but not in ZnO - its surfaces are atomically flat, stable and exhibit no reconstruction.

Applications

The applications of zinc oxide powder are numerous. Most applications exploit the reactivity of the oxide as a precursor to other zinc compounds. For material science applications, zinc oxide has high refractive index, high thermal conductivity, binding, antibacterial and UV-protection properties. Consequently, it is added into various materials and products, including plastics, ceramics, glass, cement, rubber, lubricants, paints, ointments, adhesive, sealants, pigments, foods, batteries, ferrites, fire retardants, etc

The literature was reviewed in detail, in order to gain and gather optimum information as to the genesis and the technical applications of the work and is given as follows:

The study of dilute magnetic semiconductors started in late 1960s resulted in various exciting findings. Most of the past work on DMS has focussed on (Ga, Mn) As and (In, Mn) As. But the highest reported Curie temperature (Tc) in the single phase samples grown by MBE range from ~ 35 to 172 K. This quest for a room temperature Ferromagnetic Semiconductor, gained momentum, following a theoretical prediction by Dietl et al., that ZnO and GaN would exhibit ferromagnetism above room temperature on doping with Mn, provided that the hole density is sufficiently high [8]. Several researchers have since then reported observation of room temperature ferromagnetism in doped semiconductors. A considerable attention has been paid to semiconductors doped with ferromagnetic metals (Co, Fe, and Ni). In these types of systems, the fundamental issue of much concern is that the ferromagnetic ordering could be a result of metal precipitates e.g., Co in Co doped TiO_2 and Co doped ZnO [9,10,11]. Moreover, a definite picture regarding the actual mechanism of ferromagnetic ordering in these systems has not been establishe . A ZnO based DMS would be very promising because of its widespread applications in electronic devices, such as transparent conductors, gas sensors, varistors, surface acoustic wave devices, optical wave guides, acoustooptic modulators/deflectors, ultra violet laser source, and detectors [12]. Out of all the transition metals (TM), the doping of Mn in ZnO is most favourable because Mn has the highest possible magnetic moment [13] and also the first half of the d-band is full, creating a stable fully polarized state. The theoretical studies on Mn doped ZnO also proved its novelties in the fabrication of room temperature spintronic devices**.** A T_c higher than 300 K for p-type ZnO has been predicted theoretically, but this has not been realized experimentally. Moreover, Mn is known to be anitiferromagnetic [14], which makes this system more clean in terms of metal precipitate induced ferromagnetism, which is the subject of great controversies in DMS. Despite uncertainity in the mechanism of ferromagnetism in doped semiconductors, and the fact that the obtained magnetisation is lower than the theoretically predicted value in most of the reports appearing in literature, the results reported thus far, provide a pathway for exploring the Mn doped DMS. It is however, imperative to understand the phenomenon and the factors affecting the magnetisation value in order to realize commercially applicable devices. ZnO doped with transition-metals was

experimentally reported to be no ferromagnetic for the first time in year 2001 [15]. However, after some research and development, the ZnO doped with various transition metals were often reported to be ferromagnetic either theoretically [16,17,18] or experimentally [19,20,21]. Among the doped transition metals, cobalt-doped and manganese-doped DMS have been frequently reported to be ferromagnetic. The T_c of the Co-doped ZnO is higher than that of Mn-doped ZnO. Besides the ferromagnetism above room temperature, the other properties of ZnO based DMS systems were also found similar to the typical II-VI magnetic semiconductors [22]. They have the same characteristics like absorption due to d-d transition of the doped cations, the large magnetoresistence at low temperature and the spin glass magnetic behaviours.

Thedoropoulou *et al.* **2003** [23] prepared Sn-doped ZnO were implanted with Co or Mn at doses 3–5 at.% and the implantation was performed at 350°C. The temperature-dependent magnetization measurements showed that ordering temperatures of for Co-implanted ZnO is 300K and for Mn-implanted ZnO is 250K. And there were clear hysteresis loops obtained at these temperatures. The coercive fields were < 100 Oe for all measurement temperatures. No second phases in the Mn-implanted material detection showed by X-ray diffraction .in this case origin for the ferromagnetism is a carrier-induced mechanism. The Co-implanted material showed evidence for the presence of Co precipitates with hexagonal symmetry, which is the cause of the room temperature ferromagnetism. Their results are consistent with the stabilization of ferromagnetic states by electron doping in transition metal-doped ZnO.

Panatarani *et al.* **2004 [**24**]** reported that europium doped ZnO (ZnO:Eu) particle was directly synthesized by the spray pyrolysis method. The crystal structure of samples was designated by the europium ion and the synthesis temperature. We identified the coexistence of Eu^{2+} and Eu^{3+} ions in the as prepared ZnO, which was strongly influenced by the doping concentration and the synthesis temperature. With addition of a 0.5 mol% concentration of europium ions, only the Eu^{2+} ion existed in particles, while both Eu^{2+} and Eu^{3+} ions existed in sample using 1 mol% or higher concentration of europium ions. Changing the wavelength of the excitation source, we also found that both the blue and red luminescence can be obtained.

Che *et al.* **2005** [25] prepared ZnO films by a sol–gel method. These films were characterized by X-ray diffraction (XRD) and photoluminecent spectra (PL). Effects of synthetic parameters, such as annealing atmosphere, temperature and concentration of doped ions, on the highly oriented crystal growth were studied in detail. The crystalline structures of films annealed in vacuum have wurtzite symmetry with highly c-axis orientation. A

characteristic $^5D_0 \rightarrow {}^7F_J$ (J= 1, 2, 3 and 4) red emission is observed due to energy transfer from the ZnO host to the doped Eu^{3+} in the *c*-oriented ZnO films.

Ishizumi *et al.* **2005 [**26**]** studied crystal structure, shape, and photoluminescence (PL) properties of undoped and Eu-doped ZnO nanorods. The transmission electron microscope studies show that the undoped and Eu-doped ZnO nanocrystals have the rod-like shape. Under the high energy excitation above the band-gap energy of ZnO, broad PL band as well as bound-exciton emission were observed in Eu-doped ZnO nanorods. On the contrary, several sharp PL lines were observed when the excitation energy almost coincides with the intra-4f transition energy of Eu^{3+} ions. The broad PL band is thought to be due to the defects in ZnO nanorods while the sharp PL peaks are attributed to intra-4f transitions of Eu^{3+} ions in ZnO nanorods.

Yang *et al.* **2006** [27] reported that europium doped zinc oxide (Eu:ZnO) powder has been prepared by mixing ZnO and Eu_2O_3 in deionized water and acetone solvents. The influence of phase transformation of Eu-doped ZnO powders mixed in different solvents on the luminescence behavior has been investigated. When the powder was mixed in deionized water and then sintered at high temperatures, Eu^{3+} ions were detected in the ZnO matrix. The intrinsic red photoluminescence ($^5D_0 \rightarrow {}^7F_2$) of Eu^{3+} was easily shielded by the ZnO intrinsic defect as the samples were excited with 325 nm short wavelength as a consequence of the energy level of $Eu_{Zn}^{\bullet}$ (0.19 eV) being closer to conduction band than the one of $Zn_i^{\bullet\bullet}$ (0.22 eV). Therefore, no red emission can be detected. In contrast, as the Eu-doped ZnO powder was mixed in acetone solvent (without OH^-), no Eu^{3+} ions could be detected in the ZnO matrix. In addition, the red emission could be detected not only under excitation with long wavelength (532 nm) but also at short wavelength (325 nm).

Yang *et al.* **2007** [28] reported that europium doped zinc oxide (Eu:ZnO) powder has been prepared by mixing ZnO and Eu_2O_3 in deionized water and acetone solvents. The influence of phase transformation of Eu-doped ZnO powders mixed in different solvents on the luminescence behavior has been investigated. When the powder was mixed in deionized water and then sintered at high temperatures, Eu^{3+} ions were detected in the ZnO matrix. The intrinsic red photoluminescence ($^5D_0 \rightarrow {}^7F_2$) of Eu^{3+} was easily shielded by the ZnO intrinsic defect as the samples were excited with 325 nm short wavelength as a consequence of the energy level of $Eu_{Zn}^{\bullet}$ (0.19 eV) being closer to conduction band than the one of $Zn_i^{\bullet\bullet}$ (0.22 eV). Therefore, no red emission can be detected. In contrast, as the Eu-doped ZnO powder was mixed in acetone solvent (without OH^-), no Eu^{3+} ions could be detected in the

ZnO matrix. In addition, the red emission could be detected not only under excitation with long wavelength (532 nm) but also at short wavelength (325 nm).

Mohanty *et al.* **2007** [29] reported that single crystalline Eu^{3+}-doped wurtzite zinc oxide (ZnO) nanowires were synthesized by a vapor deposition method under a controlled oxidative atmosphere. The nanowires were deposited on a Si substrate coated with 5 nm gold nanoparticles. The reaction was carried out for 30 min which resulted in high yield of vertically grown nanowires of diameter 40–150 nm and length up to several microns. The nanowires were grown along ±[0 0 0 1] direction. The concentration of dopant Eu^{3+} in the synthesized nanowires was below 1 atomic %. The crystal structure and the microstructures of the doped nanostructures were studied and compared with undoped ZnO.

Xu *et al.***2008** [30] reviewed ZnO films were prepared by pulsed laser deposition on *a*-plane sapphire substrates under N_2 atmosphere. Ferromagnetic behaviour has been obtained with the superconducting quantum interference device at room temperature and indicates a Curie temperature much above room temperature. There was no ferromagnetism was observed in intentionally Cu-doped ZnO films. This excludes that Cu doping into ZnO plays a key role in tuning the ferromagnetism in ZnO 8.8% negative magnetoresistance probed at 5 K at 60 kOe on ferromagnetic ZnO proves the lack of *s-d* exchange interaction. Anomalous Hall Effect (AHE) was observed in ferromagnetic ZnO as well as in nonferromagnetic Cu-doped ZnO films. Indicating that AHE does not uniquely prove ferromagnetism. The observed ferromagnetism in ZnO is due to intrinsic defects.

Subramanian *et al.***2009** [31] reported that synthesis and characterization of Nd doped ZnO thin films grown on Si (1 0 0) substrates by the spray pyrolysis method. The surface morphology of these thin films was investigated by scanning electron microscopy and shows the presence of randomly distributed structures of nanorods. Grazing angle x-ray diffraction studies confirm that the doped Nd ions occupied Zn sites and these samples exhibited a wurtzite hexagonal-like crystal structure similar to that of the parent compound, ZnO. The micro-photoluminescence measurement shows a decrease in the near band edge position with Nd doping in the ZnO matrix due to the impurity levels. The near-edge x-ray absorption fine structure (NEXAFS) measurements at the O K edge clearly exhibit a pre-edge spectral feature which evolves with Nd doping, suggesting incorporation of more charge carriers in the ZnO system and the presence of strong hybridization between O 2p–Nd 5d orbitals. The Nd M_5 edge NEXAFS spectra reveal that the Nd ions are in the trivalent state

Yang *et al.***2009** [32] reported that ZnO and ZnO:Eu nanorods were originally synthesized by concussion method. The nanorods present a wurtzite nanostructure with dispersive distribution morphology. The average diameter and length of the nanorods are about 80 nm and 2 lm, respectively .Other kinds of ZnO nanostructures could be obtained by this method when appropriate agents are added. However, because of the different chemical properties between trivalent rare earth ions and the cations of ZnO, it is rather difficult to incorporate rare earth ions into the lattice of semiconductors effectively via a wet chemical method. The sample of ZnO : $Eu_{1\%}^{3+}$ is single-phase and its PL signal is stronger than other singlephase ZnO : Eu_2^{3+} samples. So 1% content of Eu^{3+} was chosen as the best doping concentration.

Luo *et al.* **2010** [33] prepared europium (Eu)-doped zinc oxide (ZnO) nanocrystals by the sol–gel method. Compared with undoped ZnO nanocrystals, Eu-doped ZnO nanocrystals have enhanced ultraviolet (UV) lasing and reduced threshold at room temperature. The UV lasing properties of both the doped and the undoped samples were studied by the time-resolved and power-dependent photoluminescence (PL) experiments. The enhancement of UV lasing is due to the significantly reduced singly ionized oxygen vacancies with Eu doping, which is confirmed by both the PL spectra and the X-ray photoelectron spectra. It indicates that high-efficiency and low-threshold UV lasing sources can be fabricated from Eu-doped ZnO nanocrystals.

Devi *et al***. 2011** [34**]** prepared pure ZnO:Eu^{3+} nanoparticles (~ 50 nm) by a solution combustion method. ZnO and Eu_2O_3were used as starting materials and dissolved in nitric acid. Citric acid was used as a fuel. The reaction mixture was heated at 350 °C resulting into a rapid exothermic reaction yielding pure nanopowders. The atomic weight concentration of Eu^{3+} doped in ZnO was 20%. Transmission electron microscopy (TEM) was used to study the particle size and morphology. The nanopowders were characterized for phase composition using X-ray diffractrometry (XRD). Particle size distribution (PSD) analysis of ZnO: Eu^{3+} showed particle sizes ranging from 30 to 80 nm.The photoluminescence emission spectra of ZnO:Eu^{3+} nanostructures showed a strong band emission around 618 nm when excited with 515 nm wavelength.

So, here we will work on synthesis of Tb doped ZnO nanoparticles and will explore its properties.

3.1 GAPS IN RESEARCH

From the review of literature, it has been found that the following areas are not much explored till now. Following are the gaps in the present study:

- Study on room temperature ferromagnetism properties of rare earth doped ZnO nanoparticles.

3.2 OBJECTIVES

- ✓ The synthesis of Tb doped ZnO nanoparticles has been done using chemical co-precipitation technique.
- ✓ The characterization of Tb doped ZnO nanoparticles; structurally by X-ray diffraction (XRD), morphologically by Scanning Electron Microscopy (SEM), Transmission Electron Microscopy (TEM).
- ✓ The optical studies by Photoluminescence (PL), UV-Visible absorption spectroscopy.
- ✓ The magnetic properties by Vibrating magneto sample, Superconducting Quantum Interference Device (SQUID).

3.3 METHODOLOGY

Following steps will be taken to achieve the objectives:

- ❖ **Synthesis of Tb doped ZnO nanoparticles:** The synthesis of Tb doped ZnO has been carried out by chemical co-precipitation. In this method amount of NaOH ($4molL^{-1}$) was added $ZnCl_2$ aqueous solution with anionic surfactant SDS ($0.2molL^{-1}$) and certain volume of distilled water under strong magnetic stirring at 3 °C to get a clear solution. The solution was kept at room temperature for 1.5 h under vigorous stirring to obtain the precursor and subsequently transferred to a ground-glass stopped conical flask , aging at 85 °C for 5hr. The white products deposited on the bottom of the conical flask were collected**.**

- **Structural Analysis:** The XRD characterization will be done to know about the crystal structure, crystallinity, and phase transformation with doping.
- **Morphological Characterization**: The morphology of the synthesized product will be examined by SEM and TEM.
- **Optical analysis:** The Photoluminescence (PL) analysis and UV-visible absorption spectroscopy will be carried out to study optical transitions, defects in synthesized nanoparticles.
- **Magnetic measurements:** SQUID characterization will be performed to study the magnetic behaviour of synthesized materials

Synthesis of nano materials

There are two approaches to synthesis of nanomaterials viz Top down and Bottom up approaches as shown in figure 4.1

4.1 Top down approach

A **top-down** approach involves the division of a massive solid into smaller portions. This approach may involve milling or attrition, chemical methods, and volatilization of a solid followed by condensation of the volatilized components. Examples of top-down approach:

1. High energy milling
2. Chemical mechanical milling
3. Vapour phase condensation
4. Electro-explosion
5. Laser ablation
6. Sputtering, etc.

4.2 Bottom up approach

A bottom-up approach refers to the build-up of a material from the bottom i.e. atom by atom, molecule by molecule, or cluster by cluster. In crystal growth such as atoms, ions and molecules, after impinging onto the growth surface, assemble into crystal structure one after another. Although the bottom up approach is nothing new, it plays an important role in the fabrication and processing of nanostructure and nanomaterials. There are several reasons for this. When structures fall into a nanomaterial scale, there is little choice for top-down approach .All the tools we have possessed are too big to deal with such tiny subjects. Bottom up approach also promises a better chance to obtain nanostructures with less defects, more homogeneous chemical composition and better short and long range ordering. This is bottom-up approach is driven mainly by the reduction of gibbs free energy, so that nanostructures and nanomaterials such produced are in a state closer to a thermodynamic equilibrium state. On the contrary, top-down approach most likely introduces internal stress, in addition to surface defects and contaminations. Nanolithography or nanomanipulation is commonly a bottom-up approach. Examples of bottom-up approaches:

1. Sol-gel
2 Chemical precipitation.
3 Chemical vapour deposition
4 Self-assembly
5 Microemulsion
6 Reverse micelle

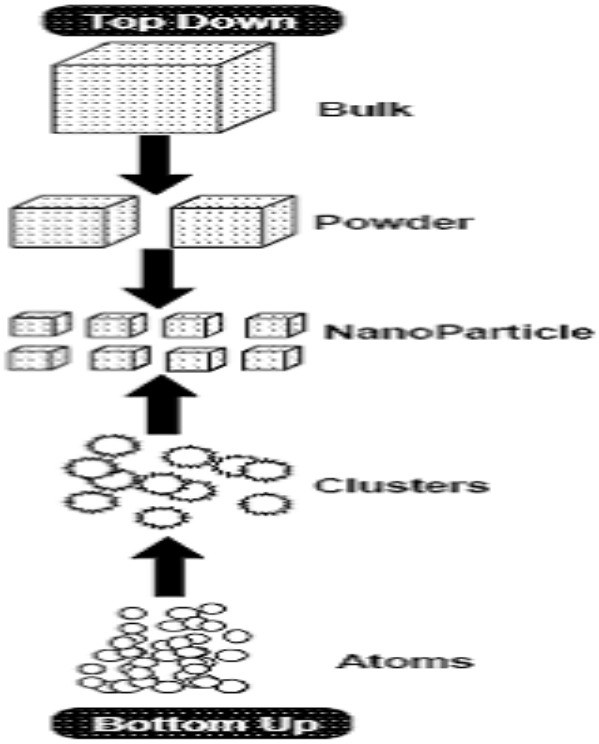

Figure4.1: Systematic of Top Down and Bottom up Approaches

4.3 Chemical co-precipitation method

The most common approach to the synthesis of colloidal nanoparticles/quantum dots is the controlled nucleation and growth in a solution of chemical precursors containing the metal and the anion sources, also called controlled arrested precipitation. Michael Faraday gave this technique by forming monodisperse gold colloids in 1857. In general, chemical precipitation means the formation of a sep- arable solid substance from a solution, either by converting the substance into an insoluble form or by changing the composition of the solvent to diminish the solubility of the substance in it. The distinction between precipitation and crystallization lies largely in whether emphasis is placed on the process by which the solubility is reduced, or on that by which the structure of the solid substance becomes organized. This technique is used industrially to remove metal ions from aqueous solutions. For example, silver ions present in a solution of a soluble salt, such as silver nitrate, are precipitated by addition of

chloride ions, provided, for example, by a solution of sodium chloride; the chloride ions and the silver ions combine to form silver chloride, a compound that is not soluble in water. For II-VI materials, solutions of chemical reagents containing the group II and VI species are rapidly mixed and homogeneously stirred. Consequently, a large number of nucleation centers are formed. Ostwald ripening, which is the growth of larger particles at the expense of smaller particles to minimize the higher surface free energy associated with particles of small size, is limited by using the surfactants/ capping agents. These surfactants/capping agents like, polyvinyl pyrrolidone (PVP) and thiophenol, form coordinating ligands in the solvent. Furthermore, pH, temperature, concentration of the surfactant, stirring speed and duration, are some of the parameters which are responsible for the resulting size distribution of the nanoparticles.

4.4 Synthesis of ZnO nanoparticles

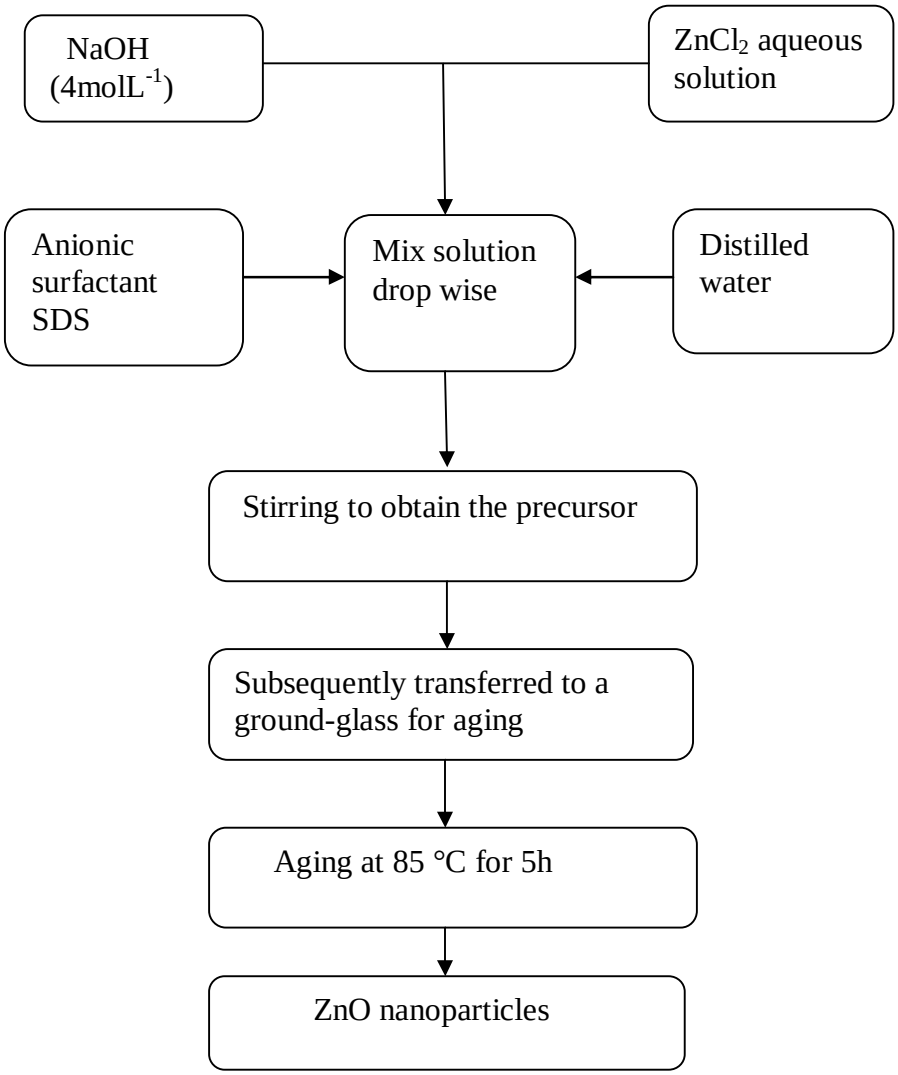

Figure4.2: Different steps involve in synthesis of ZnO

Sodium hydroxide (NaOH) and zinc chloride ($ZnCl_2$) were of analytical grade purchased from Beijing Chemical Reagent Company (China) without any further purification, and distilled water was used throughout. A typical procedure for the preparation of ZnO crystals is as follows: according to the molar ratio of Zn^{2+} to OH^-, some amount of NaOH ($4molL^{-1}$) was added drop wise into 20mL of $1molL^{-1}$ $ZnCl_2$ aqueous solution with 5mL anionic surfactant SDS ($0.2molL^{-1}$) and certain volume of distilled water under strong magnetic stirring at 3 °C to get a 100mL clear solution . After that ,the solution was kept at room temperature for 1.5 h under vigorous stirring to obtain the precursor (we called pre-stirring step) , and subsequently transferred to a ground-glass stopped conical flask , aging at 85 °C for 5h. The white products deposited on the bottom of the conical flask were collected, washed with distilled water to remove residual reactants and dried at ambient temperature. The growth process of ZnO crystals was tracked by determining the concentration of Zn (II) and the phase composition of the precipitate, which was sampled from the aging step at regular intervals. Flow chart of synthesis procedure is shown in figure4.2.

4.5 Characterization Techniques

The characterization of materials regarding determination of elemental composition, estimation of trace impurities, structural analysis, morphological analysis, dielectric analysis, magnetic analysis, identification of crystalline phases and information on crystal defects play an important role for the quality control and development of advanced materials and their use in precision devices. The nanostructures have been characterized by their structural, compositional, morphological, optical, magnetic and dielectric properties. The techniques include X-ray diffraction (XRD), Scanning electron microscopy (SEM), Transmission electron microscopy (TEM), Photoluminescence (PL), Energy Dispersive X-Ray Analysis (EDX), Superconducting Quantum Interference Device (SQUID), UV-visible Absorption Spectroscopy.

4.5.1 X-ray diffraction

XRD is a very important experimental technique that has long been used to address all issues related to the crystal structure of solids, including lattice constants and geometry, identification of unknown materials, orientation of single crystals, preferred orientation of polycrystals, defects, stresses, etc. In XRD, a collimated beam of X-rays, with a wavelength

typically ranging from 0.7 to 2 $^{\circ}$A, is incident on a specimen and is diffracted by the crystalline phases in the specimen according to Bragg's law:

$$n\lambda = 2d\sin\theta$$

where *d* is the spacing between atomic planes in the crystalline phase and λ is the X-ray wavelength as shown in figure 4.3. The intensity of the diffracted X-rays is measured as a function of the diffraction angle 2θ and the specimen's orientation. This diffraction pattern is used to identify the specimen's crystalline phases and to measure its structural properties. XRD is non-destructive and does not require elaborate sample preparation, which partly explains the wide usage of XRD method in materials characterization. Diffraction peak positions are accurately measured with XRD, which makes it the best method for characterizing homogeneous and inhomogeneous strains. Homogeneous or uniform elastic strain shifts the diffraction peak positions. From the shift in peak positions, one can calculate the change in d-spacing, which is the result of the change of lattice constants under a strain.

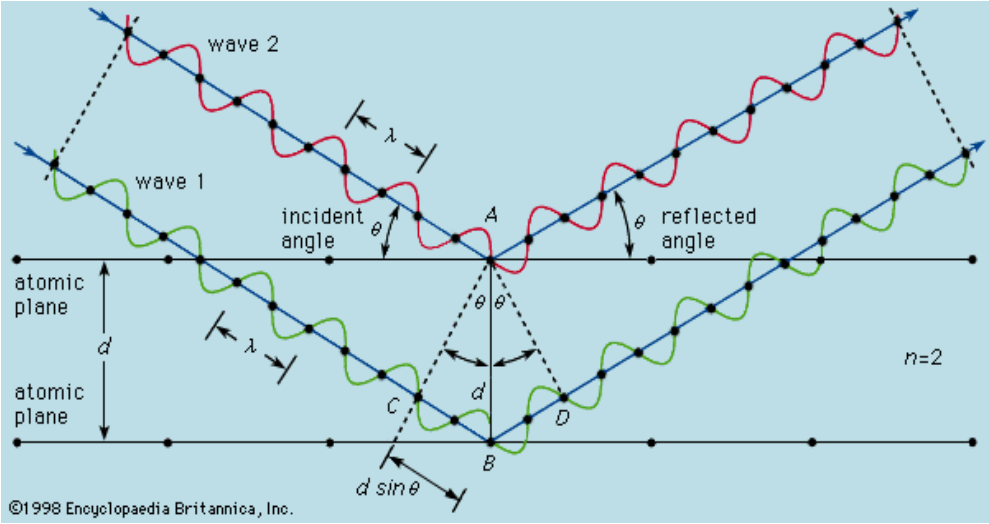

Figure 4.3 : The Bragg's law reflection, the diffracted x-rays exhibit costructive interference when the distance between paths ABC and AB'C' differs by an integer number of wavelengths (λ).

Inhomogeneous strains vary from crystallite to crystallite or within a single crystallite and this cause a broadening of the diffraction peaks that increase with sinθ**.** Peak broadening is also caused by the finite size of crystallites, but here the broadening is independent of sinθ**.**

When both crystallite size and inhomogeneous strain contribute to the peak width, these can be separately determined by careful analysis of peak shapes. If there is no inhomogeneous

strain, the crystallite size, *D,* can be estimated from the peak width with the Scherrer's formula:

$$D = K\lambda / B \cos\theta_B$$

Where λ is the X-ray wavelength, *B* is the full width of height maximum **(**FWHM) of a diffraction peak, θ_B is the diffraction angle, and *K* is the Scherrer's constant of the order of unity for usual crystal. However, one should be alerted to the fact that nanoparticles often form twinned structures; therefore, Scherrer's formula may produce results different from the true particle sizes. In addition, X-ray diffraction only provides the collective information of the particle sizes and usually requires a sizable amount of powder. It should be noted that since the estimation would work only for very small particles, this technique is very useful in characterizing nanoparticles. Similarly, the film thickness of epitaxial and highly textured thin films can also be estimated with XRD. One of the disadvantages **of** XRD, compared to electron diffraction, is the low intensity of diffracted X-rays, particularly for low-Z materials. XRD is more sensitive to high-Z materials, and for low-Z materials, neutron or electron diffraction is more suitable. Typical intensities for electron diffraction are ~ 10^8 times larger than for XRD. Because of small diffraction intensities, XRD generally requires large specimens and the information acquired is an average over a large amount of material.

It can be used to:

- Identification of unknown crystalline materials.
- Find the crystal structure of an unknown material.
- Measure the size, shape and internal stress of small crystalline regions.

4.5.2. Scanning electron microscopy (SEM) and Energy Dispersive X-Ray Analysis (EDX)

SEM is one of the most widely used techniques used in characterization of nanomaterials and nanostructures. The resolution of the SEM approaches a few nanometres, and the instruments can operate at magnifications that are easily adjusted from ~ 10 to over 300,000. Not only does the SEM produce topographical information as optical microscopes do, it also provides the chemical composition information near the surface. In a typical SEM, a source of electrons is focused into a beam, with a very fine spot size of ~5 nm and having energy ranging from a few hundred eV to 50KeV that is rastered over the surface of the specimen by deflection coils. As the electrons strike and penetrate the surface, a number of interactions occur that result in the emission of electrons and photons from the sample as shown in figure

4.4 , and SEM images are produced by collecting the emitted electrons on a cathode ray tube (CRT). Various SEM techniques are differentiated on the basis of what is subsequently detected and imaged, and the principle images produced in the SEM are of three types: secondary electron images, backscattered electron images and elemental X-ray maps.

When a high-energy primary electron interacts with an atom, it undergoes either inelastic scattering with atomic electrons or elastic scattering with the atomic nucleus. In an inelastic collision with an electron, the primary electron transfers part of its energy to the other electron.

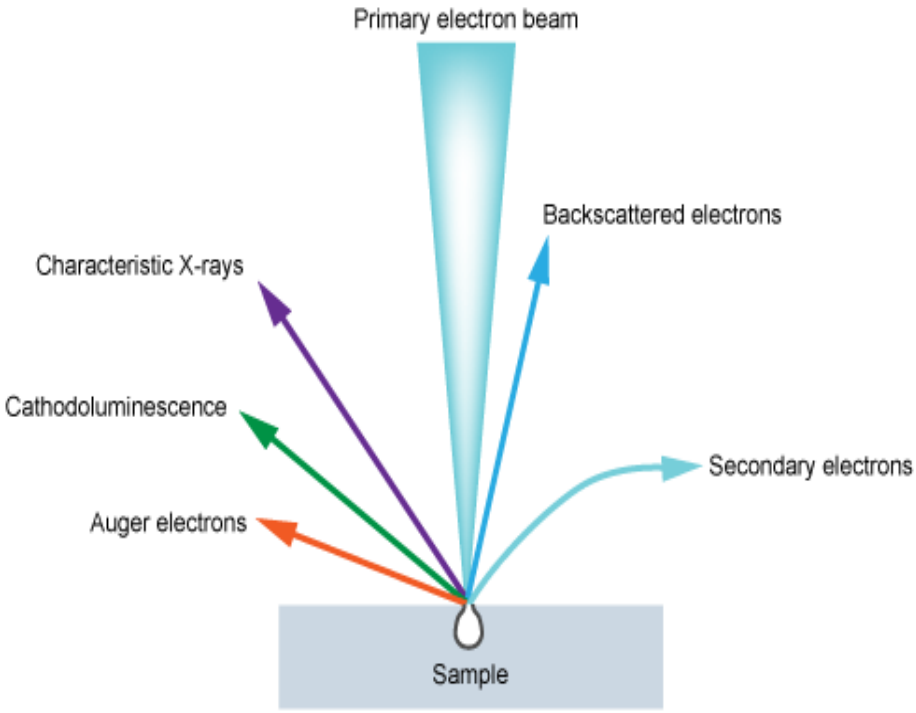

Figure 4.4: Interaction of electron with matter

When the energy transferred is large enough, the other electron will emit from the sample. If the emitted electron has energy of less than 50 eV, it is referred to as a secondary electron. Backscattered electrons are the high-energy electrons that are elastically scattered and essentially possess the same energy as the incident or primary electrons. The probability of backscattering increases with the atomic number of the sample material. Although backscattering images cannot be used for elemental identification, useful contrast can develop between regions of the specimen that differ widely in atomic number, Z. The Schematic of different component of SEM is as shown in following figure 4.5. An additional electron interaction in the SEM is that the primary electron collides with and ejects a core electron

from an atom in the sample. The excited atom will decay to its ground state by emitting either a characteristic X-ray photon or an Auger electron, both of which have been

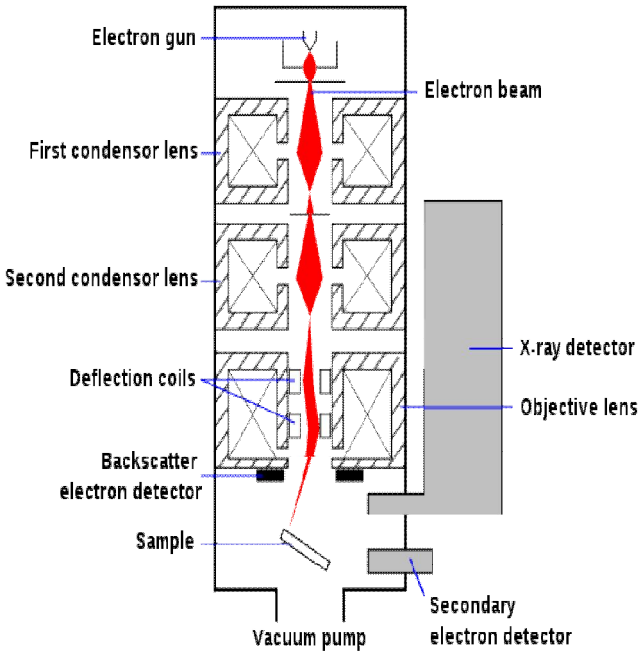

Figure 4.5: Schematic of different component of SEM

used for chemical characterization and will be discussed later in this chapter. Combining with chemical analytical capabilities, SEM not only provides the image of the morphology and microstructures of bulk and nanostructured materials and devices, but can also provide detailed information of chemical composition and distribution. The theoretical limit to an instrument's resolving power is determined by the wavelengths of the electron beam used and the numerical aperture of the system. The resolving power, *R*, of an instrument is defined as:

$$R = \lambda/2NA$$

where λ is the wavelength of electrons used and *NA* is the numerical aperture.

The SEM is routinely used to generate high-resolution images of shapes of objects and to show spatial variations in chemical compositions:

1) Acquiring elemental maps or spot chemical analyses using EDS,

2) Discrimination of phases based on mean atomic number

3) Compositional maps based on differences in trace element "activators"

4) To identify phases based on qualitative chemical analysis and/or crystalline structure.

Energy Dispersive X-Ray Analysis (EDX)

This technique is used in conjunction with SEM and is not a surface science technique. An electron beam strikes the surface of a conducting sample. The energy of the beam is typically in the range 10-20 keV. This causes X-rays to be emitted from the point the material. The energy of the X-rays emitted depends on the material under examination. The schematic of SEM and EDX is shown in figure 4.6. The X-rays are generated in a region about 2 microns in depth, and thus EDX is not a surface science technique. By moving the electron beam across the material an image of each element in the sample can be acquired.

Figure 4.6: The schematic of SEM and EDX.

Due to the low X-ray intensity, images usually take a number of hours to acquire. Elements of low atomic number are difficult to detect by EDX.When the sample is bombarded by the SEM's electron beam, electrons are ejected from the atoms comprising the sample's surface. The resulting electron vacancies are filled by electrons from a higher state, and an x-ray is emitted to balance the energy difference between the two electrons' states as shown in figure 4.7. The x-ray energy is characteristic of the element from which it was emitted. The EDS x-ray detector measures the relative abundance of emitted x-rays versus their energy. The detector is typically lithium-drifted silicon, solid-state device. When an incident x-ray strikes the detector, it creates a charge pulse that is proportional to the energy of the x-ray. The charge pulse is converted to a voltage pulse (which remains proportional to the x-ray energy)

by a charge-sensitive pre-amplifier. The signal is then sent to a multichannel analyzer where the pulses are sorted by voltage. The energy as determined from the voltage measurement, for each incident x-ray is sent to a computer for display and further data evaluation. The spectrum of x-ray energy versus counts is evaluated to determine the elemental composition of the sampled volume. The sample x-ray energy values from the EDX spectrum are compared with known characteristic x-ray energy values to determine the presence of an element in the sample.

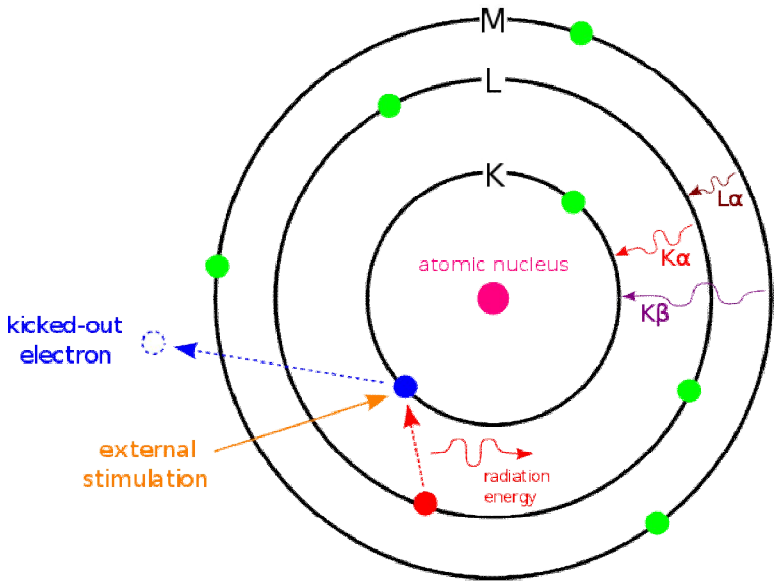

Figure4.7: The basic principle of EDX

4.5.3. Transmission electron microscopy

In TEM, electrons are accelerated to 100 KeV or higher (up to 1 MeV), projected onto a thin specimen (less than 200nm) by means of the condenser lens system, and penetrate the sample thickness either undeflected or deflected. The schematic of TEM is shown figure 4.8. The greatest advantages that TEM offers are the high magnification ranging from 50 to 10^6 and its ability to provide both image and diffraction information from a single sample. The scattering processes experienced by electrons during their passage through the specimen determine the kind of information obtained. Elastic scattering involves no energy loss and gives rise to diffraction patterns. Inelastic interactions between primary electrons and sample electrons at heterogeneities such as grain boundaries, dislocations, second-phase particles, defects, density variations, etc., cause complex absorption and scattering effects, leading to a spatial variation in the intensity of the transmitted electrons. In TEM one can switch between imaging the sample and viewing its diffraction pattern by changing the strength of the intermediate lens. The high magnification or resolution of all TEM is a result of the small effective electron wavelengths, λ, which is given by the de Broglie relationship:

$$\lambda = h / \sqrt{2mqV}$$

where m and q are the electron mass and charge, h is Planck's constant, and V is the potential difference through which electrons are accelerated. For example, electrons of 100 KeV energy have wavelengths of 0.37 nm and are capable of effectively transmitting through~0.6 μm of silicon. The higher the operating voltage of a TEM instrument, the greater its lateral spatial resolution. The schematic of TEM is as shown in the above figure. The theoretical instrumental point-to-point resolution is proportional to $\lambda^{3/4}$. High-voltage TEM instruments (with e.g. 400KV) have point-to-point resolutions better than 0.2 nm. High-voltage TEM

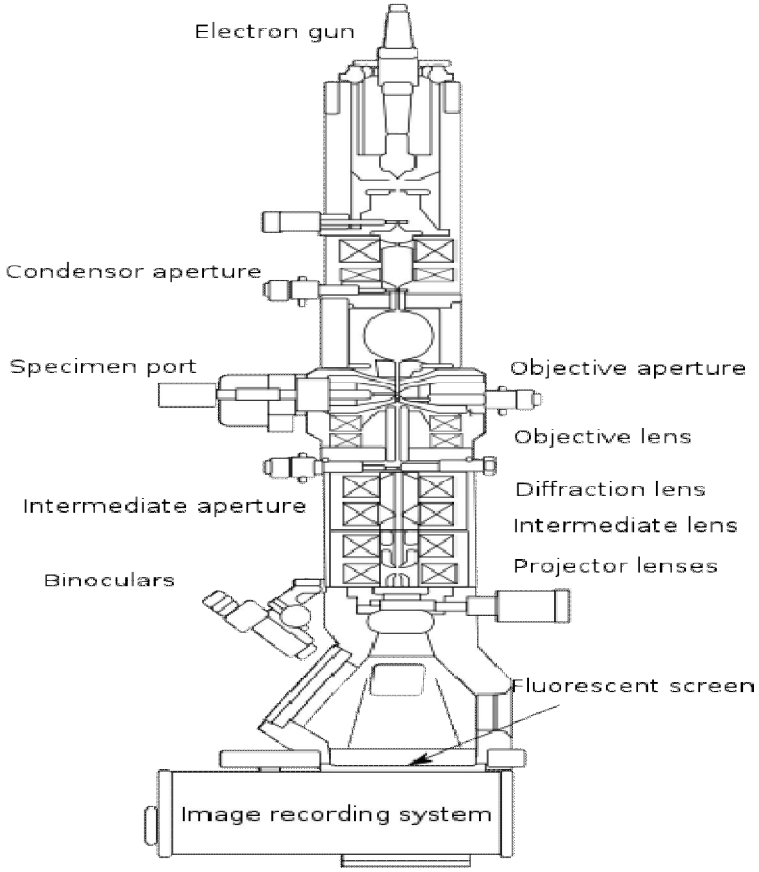

Figure4.8: Schematic of TEM

instruments have the additional advantage of greater electron penetration, because high-energy electrons interact less strongly with matter than lower energy electrons. So it is possible to work with thicker samples on a high voltage TEM. One shortcoming of TEM is its limited depth resolution. Electron scattering information in a TEM image originates from a three dimensional sample, but is projected onto a two-dimensional detector. Therefore, structure information along the electron beam direction is superimposed at the image plane.

Although the most difficult aspect of the TEM technique is the preparation of samples, it is less the crystal structure of individual nanomaterials, such as nanocrystals and nanorods, and the crystal structures of different parts of a sample.

4.5.4. Photoluminescence

Luminescence refers to the emission of light by a material through any process other than blackbody radiation. The emission of light can result from a variety of stimulations. For example, when the emission is resulted from electronic stimulation, it is referred to as cathodoluminescence (CL). Another example is X-ray fluorescence, when high-energy photons, i.e. X-ray, are used to excite the sample. In PL one measures physical and chemical properties of materials by using photons to induce excited electronic states in the material system and analyzing the optical emission as these states relax. Typically, light is directed onto the sample for excitation, and the emitted luminescence is collected by a lens and passed through an optical spectrometer onto a photon detector. The spectral distribution and time dependence of the emission are related to electronic transition probabilities within the sample.

We get Quantitative information from PL about:

1. Chemical composition.
2. Structure, impurities.
3. Kinetic process. And Energy transfer.

Sensitivity is one of the strengths of the PL technique, allowing very small quantities (nanograms) or low concentrations (parts-per-trillion) of material to be analyzed. Precise quantitative concentration determinations are difficult unless conditions can be carefully controlled, and many applications of PL are primarily qualitative. In PL, a material gains energy by absorbing photon at some wavelength by promoting an electron from a low to a higher energy level. This may be described as making a transition from the ground state to an excited state of an atom or molecule, or from the valence band to the conduction band of a semiconductor crystal or polymer (electron-hole creation). The system then undergoes a non-radiative internal relaxation involving interaction with crystalline or molecular vibrational and rotational modes, and the excited electron moves to a more stable excited level, such as the bottom of the conduction band or the lowest vibrational molecular state. After a characteristic lifetime in the excited state, electron will return to the ground state. In the luminescent materials some or all of the energy released during this final transition is in the

form of light, in which case the relaxation is called radiative. The wavelength of the emitted light is longer than that of the incident light. It should be noted that depending on the characteristic life-time of emission, fast PL with life-time of sub-microsecond is also called "fluorescence", whereas slow ones, 10^{-4} to 10 s, are referred to as "phosphorescence" .Optical absorption and photoluminescence spectra are commonly used in the characterization of the size of nanocrystals of semiconductors.

4.5.5. Superconducting Quantum Interference Device

The SQUIDS is the most sensitive devices for the detection of magnetic flux. They have been used in a wide range of applications, such as susceptometry, nuclear magnetic resonance, non-destructive evaluation, biomagnetism, scanning SQUID microscopy, etc. Other possible applications that have been suggested include the storage of electrical energy without loss, the building of superconducting computers, non invasive measurement of internal fruit quality, etc. Although low-temperature (low-T_c) SQUIDs are being used in the above applications, the invention of high-temperature superconductors (materials of which the critical temperature is in the region of 100K) makes the fabrication and application of these devices more feasible.The measurement of the flux change through a pick-up coil system with a SQUID. This signal is proportional magnetic moment of a sample which is magnetized by the magnetic field produced by a superconducting magnet. The main components of a SQUID magnetometer are: (a) superconducting magnet (that must be acquired together its programmable bipolar power supply); (b) superconducting detection coil which is coupled inductively to the sample; (c) a SQUID connected to the detection coil. (d) Superconducting magnetic shield. High sensitivity is possible because this device responds to a fraction of the flux quantum. The SQUID device is usually a thin film that functions as a extremely sensitive current-to-voltage-converter.

A measurement is done in this equipment by moving the sample through the second-order gradiometer. Hence, the magnetic moment of the sample induces an electric current in the pick-up coil system. A change in the of magnetic flux in these coils changes the persistent current in the detection circuit. So, the change in the current in the detection coils produce variation in the SQUID output voltage proportional the magnetic moment of sample. The superconducting magnetic shield is used to shield the SQUID sensor from the fluctuations of the ambient magnetic field of the place where the magnetometer is located and from the large magnetic field produced by the superconducting magnet.

Applications

- The real and imaginary components of the AC magnetic susceptibility as a function of frequency, temperature, AC magnetic field amplitude and DC magnetic field value.
- The DC magnetic moment as a function of temperature, DC magnetic field, and time. Using a specially designed sample holder the magnetic moment as a function of angle can be also measured.

4.5.6. UV-visible Absorption Spectroscopy

UV-vis spectroscopy is the measurement of the wavelength and intensity of absorption of near-ultraviolet and visible light by a sample. Ultraviolet and visible light are energetic enough to promote outer electrons to higher energy levels. UV-vis spectroscopy is usually applied to molecules and inorganic ions or complexes in solution. The UV-vis spectra have broad features that are of limited use for sample identification but are very useful for quantitative measurements. The concentration of an analyte in solution can be determined by measuring the absorbance at some wavelength and applying the The Beer-Lambert law (or Beer's law)

It is the linear relationship between absorbance and concentration of an absorbing species.

The general Beer-Lambert law is usually written:

$$A = a(\lambda) * b * c$$

where A is the measured absorbance, $a(\lambda)$ is a wavelength-dependent absorptivity coefficient, b is the path length, and c is the analytic concentration. When working in concentration units of molarity, the Beer-Lambert law is written as:

$$A = \varepsilon * b * c$$

where ε is the wavelength-dependent molar absorptivity coefficient with units of M^{-1} cm^{-1}.

Experimental measurements are usually made in terms of transmittance (T), which is defined as:

$$T = I / I_o$$

where I is the light intensity after it passes through the sample and I_o is the initial light intensity.The relation between A and T is given by:

$$A = -\log T = -\log (I / I_o)$$

Modern absorption instruments can usually display the data as transmittance, % transmittance, or absorbance. An unknown concentration of an analyte can be determined by measuring the amount of light that a sample absorbs and applying Beer's law.

5.1 Structural analysis

Figure 5.1 shows the XRD pattern of pure ZnO and Tb-doped ZnO nanoparticles for x=0.02 and x=0.04 respectively. All the peaks were found to correspond to the wurtzite structure of zinc oxide exhibit hexagonal phase with primitive unit cell and space group $P6_3mc$ (JCPDS file no. 800075). It is predicted from Fig.5.1 that the peaks positioned at 69.26^0 and 77.09^0 corresponds to Tb_2O_3 with body centred phase (JCPDS file no. 23-1419). It is also clearly depicted from Fig. 5.1 that doping of Tb does not change the wurtzite structure of ZnO.

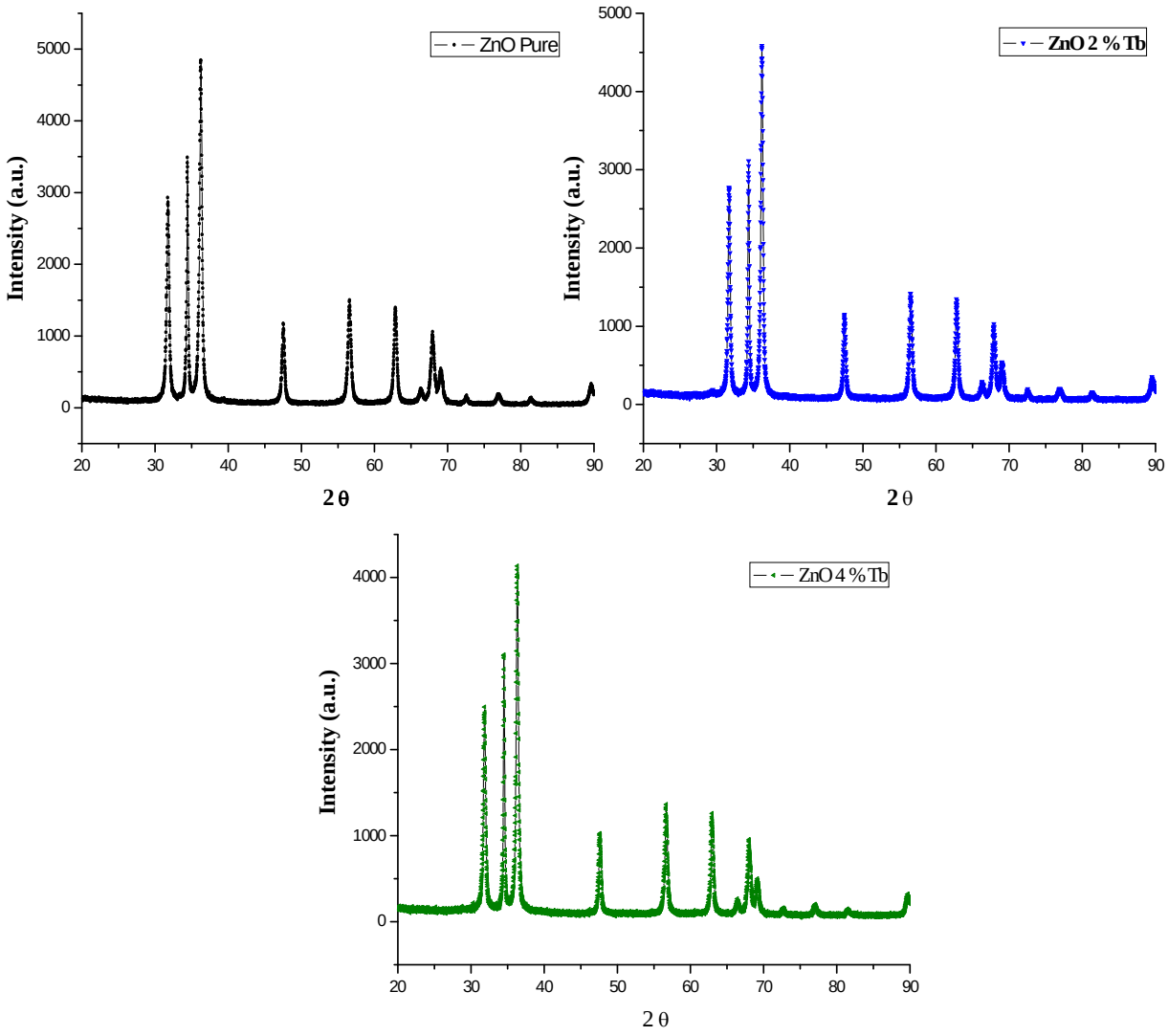

Figure 5.1: The XRD pattern of ZnO nanoparticles (a) pure (b) doped with 2 % and (c) 4% Tb

The XRD peaks were sharp and highly intense indicating the high crystallinity nature of ZnO nanoparticles. The average crystallite size on ZnO nanoparticles is measured by Debye-Scherer's fomula

$$B/\lambda = 1/L + \varepsilon \sin\theta/\lambda \quad (1)$$

where β is FWHM, L is crystallite size, θ angle of diffraction, and ε is micro-strain. The average crystallites size found to be 26 nm for pure samples and it increase to 32 nm and 43 nm with 2% and 4% doping of Tb in ZnO. It has been noticed that the addition of Tb atoms in ZnO nanoparticles contribute some strain as they substitute for Zn. The stain values obtained from Williamson-hall plot (eqn. 1) is very small and their effect on broadening is negligible.

5.2 Morphological analysis

5.2.1 TEM analysis

Figure 5.2(a) represents the TEM image of 2% Tb doped ZnO nanoparticles calcined at 350^{o}C . The particles were found to be almost spherical in shapes. A statistical analysis reveals that the mean particle sizes are approximately 100 nm for 2 % Tb doped ZnO.

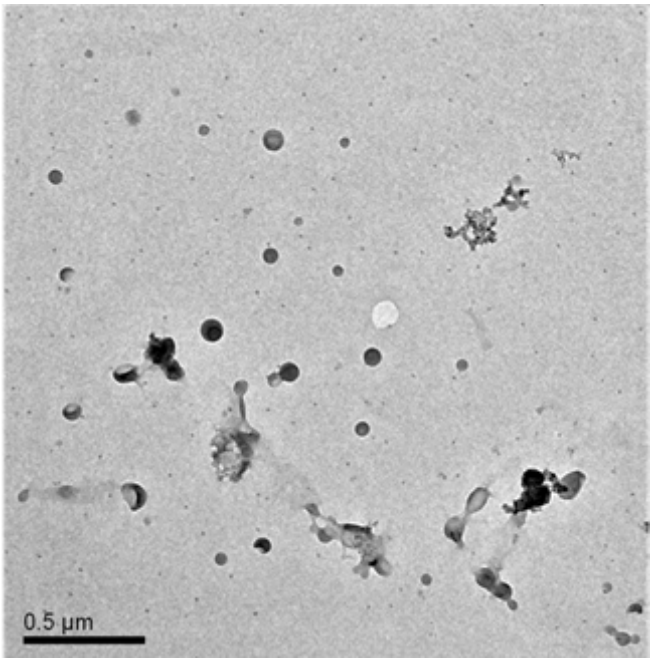

Figure 5.2 The TEM image of ZnO nanoparticles doped with 2% Tb

5.2.1. SEM and EDX study

The SEM micrographs of pure and 2% Tb doped ZnO nanoparticles is shown in figure 5.3 The morphology of pure ZnO particles seemed to be approximately spherical in shape. But

however with 2% Tb doping leads to particles nearly spherical in shape with grain size 500 nm.

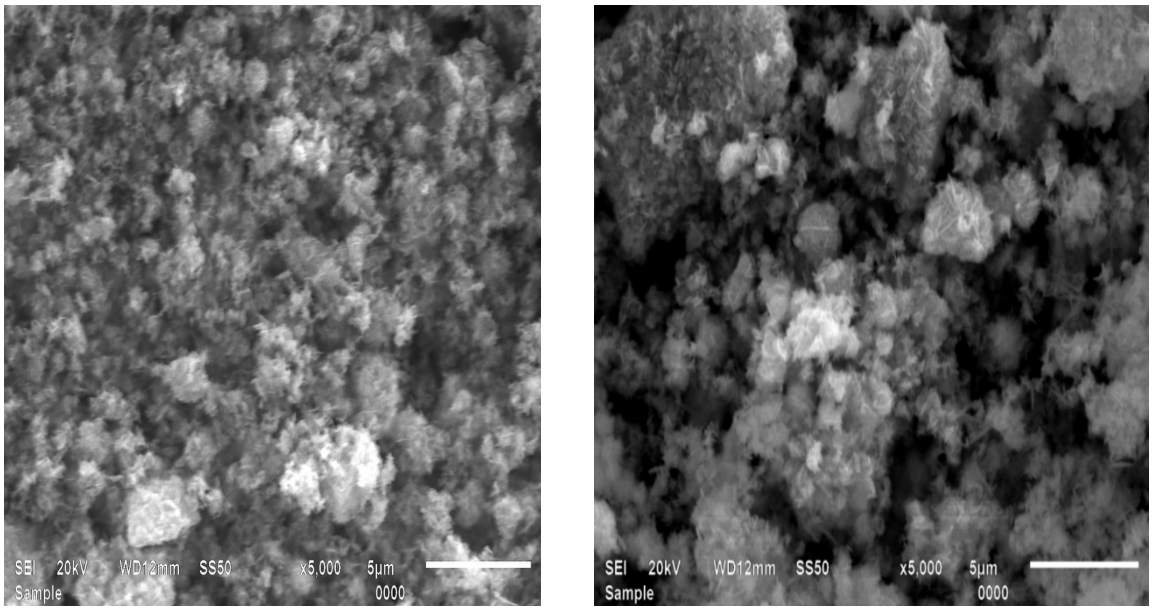

(a) (b)

Figure 5.3: SEM micrographs of (a) pure and (b) 2% Tb doped ZnO

The Chemical composition of the nanoparticles was analysed by energy dispersive x-ray (EDX) spectra of pure ZnO and 2% Tb-doped ZnO nanoparticles are shown in figure 5.4
It is clear from figure 5.6 that Zn and O are in stoichiometric ratio and therefore indicates the formation of pure ZnO.

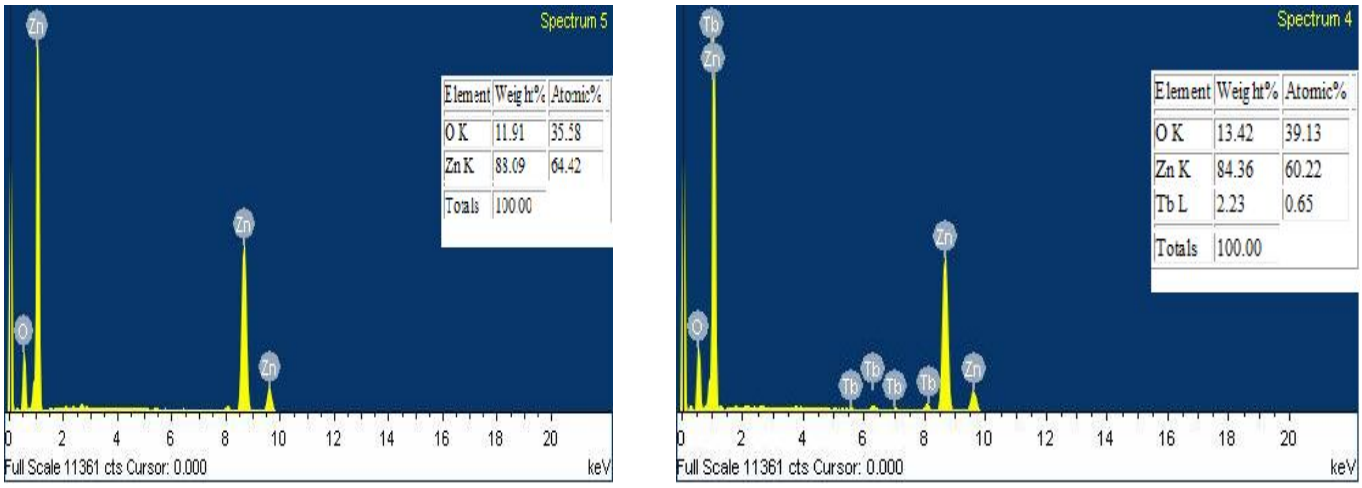

(a) (b)

Figure 5.4 EDX spectra of (a) pure and (b) 2% Tb doped ZnO

5.3. Optical analysis

Figure 5.5 shows the optical absorption spectra for the pure, 2% and 4% Tb doped ZnO nanoparticles.

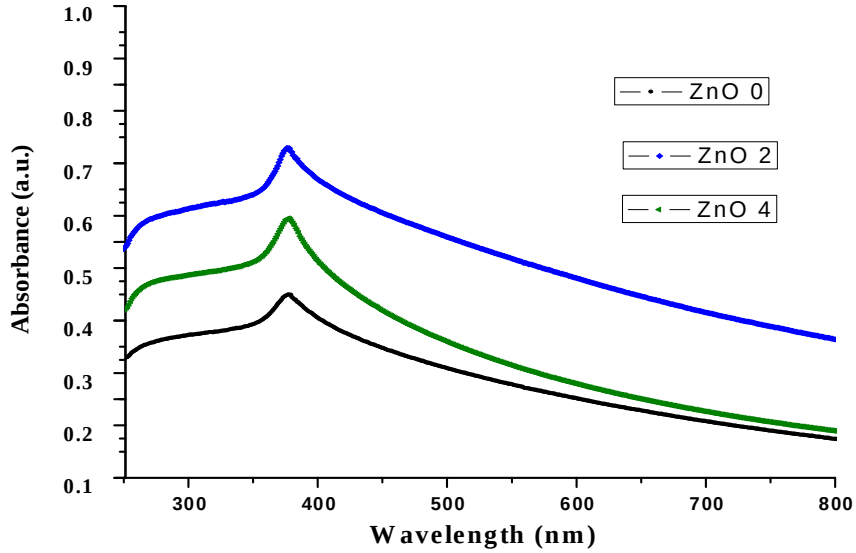

Figure 5.5 The UV-Visible absorption spectra of (a) pure, (b) 2% Tb doped and, (c) 3% Tb doped ZnO nanoparticles.

It is clear from Fig. 5.5 that the absorption edge is around 375nm for pure ZnO and it increases with addition of 2 % and 4% Tb respectively to 377nm and 378nm. The corresponding band gap calculated using Tauc's relation found to be 3.31, 3.29, 3.28 eV resp. for pure, 2% and 4% Tb doped ZnO nanoparticles. It is clear from the absorption study that no blue shift in the optical band gap found. This can be attributed due the fact that the particles size of ZnO nanoparticles is greater than bohr exciton radius of ZnO and hence no shift in band gap observed.

5.4. Magnetic analysis

Figure 5.6 shows the magnetization versus magnetic field *M-H* loops for the, pure ZnO and Tb doped ZnO nanoparticles. The pure ZnO nanoparticles shows ferromagnetic behaviour with very small magnetic saturation field value ~ 1.35×10^{-5} emu/g. But it is clear that with addition of Tb metal, the Tb doped ZnO nanoparticles shows antiferromagnetic behaviour as no magnetic field saturation observed. The occurrence of ferromagnetic behaviour in pure ZnO nanoparticles may be attributed due to the defects like oxygen or cation vacancies [8]. The remnant magnetisation m_r is 2.69×10^{-5} emu/g and coercive field is 2019.43 Oe observed for pure ZnO nanoparticles. With Tb doping, defects concentration reduces and ZnO: Tb show antiferromagnetic behaviour.

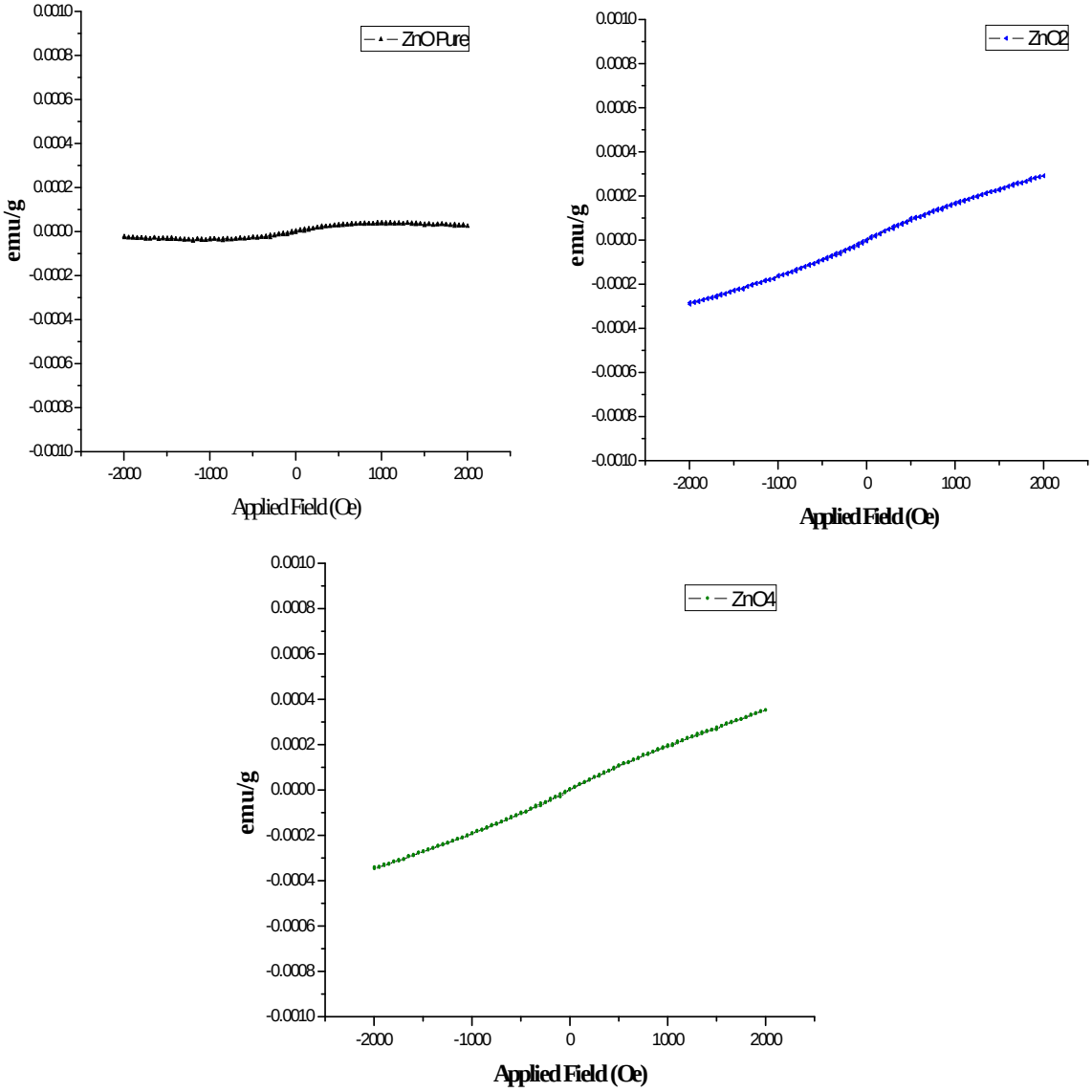

Figure 5.6 The magnetization versus magnetic field, *M-H* loops for (a) pure (b) 2% and (c) 4 % Tb doped ZnO nanoparticles

5.6 Conclusion

In this Tb doped ZnO nanoparticles were successfully synthesized by co-precipitation technique. The influence of Tb doping on structural, optical and magnetic properties were studied.

- Tb doped ZnO nanoparticles were successfully synthesized by co-precipitation technique.
- All the peaks were found to correspond to the wurtzite structure of zinc oxide exhibit hexagonal phase with primitive unit cell. The peaks positioned at 69.26^0 and 77.09^0 correspond to Tb_2O_3 with body centred phase and doping of Tb does not change the wurtzite structure of ZnO. The average crystallites size found to be 26 nm for pure samples and it increase to 32 nm and 43 nm with 2% and 4% doping of Tb in ZnO.
- It has been noticed that the addition of Tb atoms in ZnO nanoparticles contribute some strain as they substitute for Zn.
- The morphology of pure ZnO particles seemed to be approximately spherical in shape. But however with 2% Tb doping leads to particles nearly spherical in shape with grain size 500 nm.
- The pure ZnO nanoparticles shows ferromagnetic behaviour with very small magnetic saturation field value ~ 1.35×10^{-5} emu/g. But it is clear that with addition of Tb metal, the Tb doped ZnO nanoparticles shows antiferromagnetic behaviour as no magnetic field saturation observed. The occurrence of ferromagnetic behaviour in pure ZnO nanoparticles may be attributed due to the defects like oxygen or cation vacancies.

References

[1] Dielt.T,Ohno.H, Matsukura.F, Cibert.J ,Ferrand.D, Science **287,**(2000),1019

[2] Dietl.T, Semicond. Sci. Technol **17,**(2002), 377

[3] Pearton.J.S, Heo W.H, Ivill.M, Norton D.P, Steiner.T, Semicond. Sci Technol **19,**(2004),59

[4] Dietl.T, Matsukura.F, Ohno.H, Phys.Rev **B66,**(2002), 033203

[5] Litvinov V.I,Dugaev V.K, Phys. Rev. Lett **86,**(2001),5593

[6] Sarma D.S,Hwang E.H ,Kaiminski.A, Phys. Rev **B67,**(2003),155201

[7] Wolf S.A,Awschalom D.D, Buhrman R.A, Daughton J.M ,Molnar S.V,Roukes L.M, Chtchelkanova A.Y,Treger D.M , Science**294,**(2001),1488

[8] Zajac.M, Doradzinski.R, Gosk.J, Szczytko.J, Lefeld- Sosnowska .M, Kaminska .M, Twardowski .A, Palczewska.M, Grzanka .E, Gebicki .W, Appl. Phys. Lett **78,**(2001), 1276

[9] Alberta Bonanni, Michal Kiecana, Clemens Simbrunner, Tian Li, Maciej Sawicki, Matthias Wegscheider, Martin Quast, Hanka Przybylińska, Aandrea Navarro-Quezada, Rafal Jakiela, Agnieszka Wolos, Wolfgang Jantsch, and Tomasz Dietl, Phys. Rev**B75,**(2007), 125210

[10] Zajac.M, Gosk .J, Grzanka.E, Kaminska .M , Twardowski.A , Strojek .B, Szyszko.T, Podsiadlo .S, J.Appl Phys **93,**(2003), 4715

[11] Sonoda .S, Tanaka.I, Ikeno .H, Yamamoto .T, Oba .F, Araki .T,Yamamoto .Y, Suga .K, Nanishi .Y, Akasaka .Y, Kindo .K, Hori .H, J. Phys **18,**(2003), 4615

[12] Das .G.P, Rao .B.K, Jena .P, Phys. Rev **B68,**(2003), 035207

[13] Biswas .K, Sardar .K, Rao .C.N.R, Appl. Phys. Lett. **89,**(2006), 132503

[14] Venkatesan .M, Fitzgerald .C.B, Coey .J.M.D, Nature_London **430,**(2004), 630

[15] Ando.K,Saito.H, Jin.Z, Fukumura.T,Kawasaki.M, Matsumoto.Y, Koinuma.H, *Appl.* Phys. Lett.**78,***(* 2001), 2700

[16] Sluiter M.H .F,Kawazoe.Y, Sharma.P, Inoue.A, A. Raju.R, Rout.C , Maghmare U.V, Phys. Rev. Lett.**B94,**(2005), 187204

[17] Huang L.M, Rosa A.L,Ahuja.R, Phys. Rev**B74**,*(*2006), 075206

[18] Risbud A.S, Spaldin N.A, Chen Z.Q, Stemmer.S , Seshadri.R, Phys. Rev **B68,**(2003), 205202

[19] Tuan A.C, Bryan J.D, Pakhomov A.B, Shutthanandan.V, Thevethasan.S, McCready D.E, Gaspar.D, Engelhard M.H, Rogers J.W, Krishnan J.K, Gamelin D.R, Chambers S.A, Phys. Rev **B70,**(2004), 054424

[20] Norton D.P, Overberg M.E, Pearton S.J, Pruessner.K, Budai J.D, Boatner L.A, Chisholm M.F,Lee J.S, Khim Z.G, Park Y.D,Wilson R.G,

Appl. Phys. Lett **83**,(2003), 5488.

[21] Rode.K, Anane.A, Mattana.R, Contour J.P, Durand.O,LeBourgeois.R, J. Appl. Phys **93**, (2003), 7676

[22] Jin.Z,Fukumura.T, Kawasaki.M, Ando.K, Saito.H, Sekiguchi.T, Yoo Y.Z, Murakami.M, Matsumoto.Y, Hasegawa.T , Koinuma.H, Appl. Phys. Lett **78**,(2001), 3824

[23] Theodoropoulou N.A , Hebard A.F , Norton D.P, Budai J.D,Boatner L.A , Lee d J.S, Khim Z.D, Park Y.D, Overberg M.D,Pearton S.J,Wilson R.G , Solid-State Electronics **47**,(2003),2231

[24] Panatarani.C, Wuled.I, Lenggoro, Okuyama.K, J. Appl. Phys **65**,(2004),1843

[25] Che.P, Meng.J, Guo.L Institute of Applied Chemistry **486**,(2005), 50

[26] Ishizumi.A, Taguchi.Y, Yamamoto.A, Kanemitsu.Y J.Luminescence **30**,(1998), 87

[27] Yang C.C, Cheng S.Y,Lee H.Y,Chen S.Y, Ceramics International **32,**(2006),37

[28] Yang C.C, Cheng S.Y,Lee H.Y , Chen S.Y, Chemical Physics Letters **440**,(2007), 121

[29] Mohanty.P,Kim.B, Park.J, Materials Science and Engineering **B138,**(2007),224

[30] Xu.Q, Schmidt.H, Zhou.S, Potzger.K, Helm.M, Hochmuth.H, Lorenz.M, Setzer.A, Esquinazi.P, Meinecke.C, Grundmann.M, J.App Phys **92**, (2008), 082508

[31]Subramanian.M, Thakur.P, Gautam.S, Chae, K.H, Tanemura1.M, Hihara.T, Vijayalakshmi.S, Soga1.T, Kim S.S, Asokan.K, Jayavel.R J.Phys **D 42** ,(2009),105410

[32] Yang.Y, Lai H.E,Tao E.C , Yang E.H, J Mater Sci **21,**(2010),173

[33] Luo.L,Gong.L,Liu Y.F, Chen.J[c], Ding C.R,Tang Y.G, Li X.L, Qiu Z.R, Wang H.Z, Chen X.M, Li K.F, Fan H.H, Cheah K.W,Opt Materials **32,**(2010),1066

[34] Devi S.K.L, Kumar K.S,Balakrishnan.A, Dep. of Physics **65,**(2011), 35

[35] H. Ohno et al., Nature **408**, (2000) 944

[36] A. Oiwa et al., Phys. Rev. Lett. **88**, (2002) 137202

[37] T. Dietl et al., Science **287**, (2000) 1019

[38] Petersen et al., J. Appl. Phys. **107**, (2010) 123522

[39] Yang et al. J. Nanopart. Res. **12** ,(2010) 217

[40] Kale et al. Semicond. Sci. Technol. 19 (2004) 980

[41] Xie et al., J. Phys. Chem. Solids. **70**, (2009) 112

[42] Panchakarla et al., Chem. Phys.Chem. **11**(2010) 1673.